Synthesis, redox chemistry and solid state structure of di- and trinuclear ferrocenyl substituted N-alkylpyrazolyl pyridine complexes

Werner R. Thiel [a,*], Thomas Priermeier [a], Dirk A. Fiedler [a], Alan M. Bond [b], Mike R. Mattner [a]

[a] *Anorganisch-chemisches Institut, Technische Universität München, Lichtenbergstraße 4, D-85747 Garching, Germany*
[b] *Chemistry Department, Monash University, Clayton, Vic. 3168, Australia*

Abstract

Di- and trinuclear transition metal complexes were obtained by the reaction of ferrocenyl substituted pyrazolyl pyridines with $Mo(CO)_4(pip)_2$ (pip = piperidine, **5**). The structure of the dinuclear complex tetracarbonyl{[5-ferrocenyl-3-(2-pyridyl)-1-pyrazolyl]aceticacidethylester}molybdenum(0), **6a**, was determined by X-ray structure analysis. The redox properties of the complexes were characterized by cyclovoltammetry. The shifts in reversible potential, observed when the molybdenum tetracarbonyl and ferrocene moieties are attached to the ligand system, were consistent with changes observed in spectroscopic parameters.

Keywords: Ferrocene; Carbonyl complexes; Cyclovoltammetry; X-ray structure

1. Introduction

Oligonuclear ferrocenyl substituted complexes have recently attracted attention owing to their catalytic potential [1]. Additionally, the study of metal-metal interactions and the redox chemistry associated with suitable model complexes may also be anticipated to lead to a better understanding of electron transfer reactions of metallo enzymes where electrons can be transported over very large distances. Ferrocene derivatives commonly show reversible oxidation ($Fc^{+/0}$). If the ferrocene redox potential is comparable with potentials exhibited in biological systems, model complexes of ferrocene linked by a ligand system to another metal centre can be proposed as providing a model of an electrochemical probe of the electron transfer process in biologically important molecules [2].

At present, several chelating donor ligands containing a conjugated ferrocenyl fragment have been de-scribed in the literature [3]. In principle, these systems should allow electron transfer between the ferrocene and another coordinated metal centre via the ligand backbone. This would then represent the kind of compound that is a likely candidate for a model of the electron transfer.

Pyrazolyl pyridine [4] has already been shown to provide a convenient system for the study of ligand effects in catalysis, since a wide range of derivatives of the ligand is readily accessible. Application of these ligands for catalytic olefin epoxidation with molybdenum peroxo complexes was a matter of research in one of our groups [5]. Coupling of ferrocene to a metal complex could then be expected to provide a system, which would exhibit a well-defined and interesting electron transfer chemistry.

In 1965, Wolf and Hennig described the synthesis of 1-ferrocenyl-3-pyridylpropan-1,3-diones and the related pyrazoles [6]. However, the coordination chemistry of these redox active N,N'-donor ligands is not yet known. In this paper the redox chemistry of this ferrocenyl-N,N'-donor ligand and its coordination to a molybdenum tetracarbonyl fragment are described. The molybdenum tetracarbonyl group, like ferrocene, can be read-

---

* Corresponding author.

ily oxidized [7], so shifts in potential depending on the presence of the coordinated metal centre and ligand can be revealed.

2. Results and discussion

2.1. Syntheses

Pyrazoles are generally obtained by 2 + 3 cycloaddition of a diazo compound with an acetylene or by ring closure reaction of hydrazine with a 1,3-diketone [8], which can be obtained by Claisen-condensation. We started with acetyl ferrocene (1a) or diacetyl ferrocene (1b) (Schemes 1 and 2). Claisen-condensation with ethyl picolinate in liquid ammonia gave the 1,3-diketones 2a,b, which were directly reacted with aqueous hydrazine in ethanol, leading to the pyrazolyl pyridine substituted ferrocenes 3a,b in about 50% overall yield. As a consequence of the low solubility of bipyridine or pyrazolyl pyridine transition metal complexes, alkylation of N1 with ethyl bromoacetate was carried out. The alkylated pyrazolyl pyridines 4a,b are now highly soluble even in nonpolar solvents like n-hexane.

A convenient starting material for the synthesis of a wide range of tetracarbonylmolybdenum(0) complexes is cis-Mo(CO)$_4$(pip)$_2$ (pip = piperidine, 5). The weakly bonded piperidine can easily be exchanged by phosphorus and nitrogen donor ligands [9]. The reaction of one or two equivalents of 5 with the chelating ferrocene ligands 4a,b in toluene led respectively to the di- and trinuclear carbonyl complexes 6a,b, which were obtained as orange-red crystalline solids (Scheme 3). In an analogous reaction, the unsubstituted ligand [3-(2-pyri-
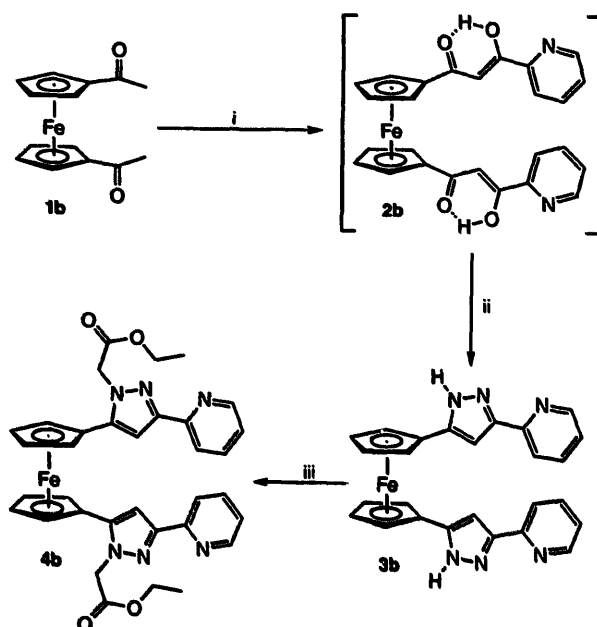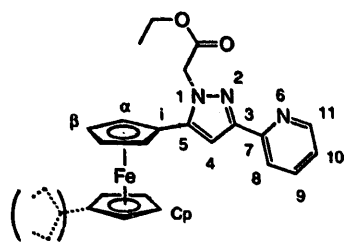

Scheme 2. (i) KNH$_2$–NH$_3$, ethyl picolinate–Et$_2$O, −35 to 25 °C, CH$_3$COOH; (ii): N$_2$H$_4$–EtOH, reflux; (iii): THF, NaH, BrCH$_2$COOEt, 25 °C.
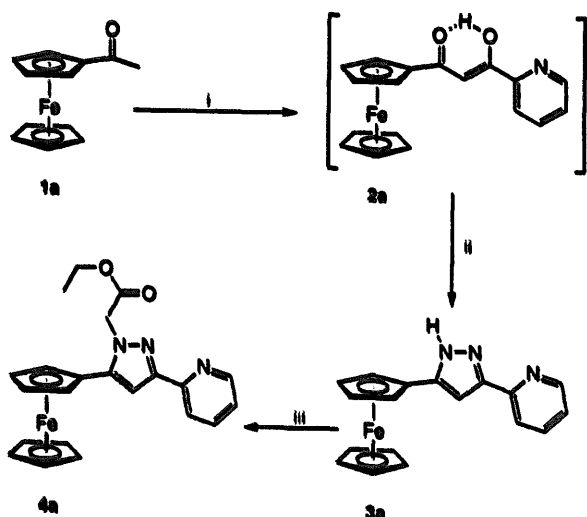
Scheme 1. (i): KNH$_2$–NH$_3$, ethyl picolinate–Et$_2$O, −35 to 25 °C, CH$_3$COOH; (ii): N$_2$H$_4$–EtOH, reflux; (iii): THF, NaH, BrCH$_2$COOEt, 25 °C.
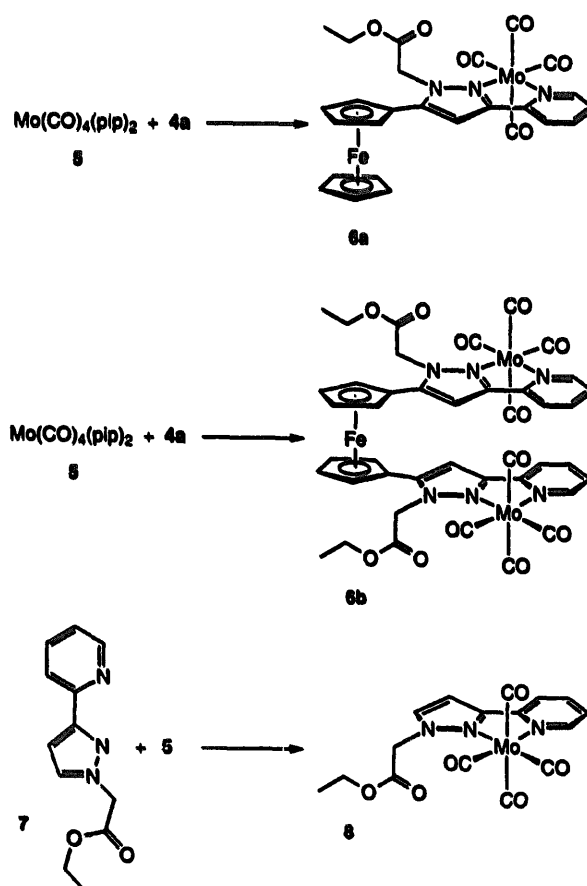
Scheme 3.

Scheme 4.

dyl)-1-pyrazolyl]aceticacidethylester (7) [5a] was converted into 8.

2.2. Spectroscopy

All compounds were characterized by IR and NMR spectroscopy. The ferrocenyl protons of compounds 3a,b, 4a,b, and 6a,b were assigned by steady state NOE experiments.

An absorption in the IR spectrum (KBr) of the ferrocenylpyrazolyl pyridine 3a at 3234 cm^{-1} can be assigned to the NH stretching mode. This absorption shifts to 3104 cm^{-1} in the case of the disubstituted compound 3b, which indicates the formation of strong intra-/intermolecular H-bonds. These bonds are responsible for the drastically reduced solubility of 3b compared with 3a. Protonation with aqueous HCl leads to a deep red solution. ^{1}H NMR investigations on this solution show a low field shift of the pyridinic protons and a slight high field shift of the pyrazolic proton. These observations indicate that protonation of the pyridinic nitrogen has occurred, which can be explained by the higher basicity of the pyridine moiety compared with the pyrazole moiety.

The CO stretching modes of carbonyl complexes of type (L-L)Mo(CO)$_4$ are influenced by the electronic properties of the donor ligands [10]. Ferrocenyl substituted (6a,b), as well as the unsubstituted (8), Mo(CO)$_4$ complexes show the same CO absorptions within experimental accuracy in both toluene solution and solid state (KBr). Therefore, the electronic influence of the ferrocenyl substituent on the heteroaromatic system and on its coordination chemistry is weak, which is corroborated by electrochemical data. The mono- and disubsti-

tuted ferrocenyl ligands 4a and 4b and the unsubstituted ligand [3-(2-pyridyl)-1-pyrazolyl]aceticacidethylester (7) [5a] show almost the same resonances in the ^{1}H NMR; however, the carbonyl complexes 6a and 6b give different resonances for the pyrazolyl pyridine moieties (the NMR spectra were assigned according to Scheme 4). The resonances are shifted by 0.28 ± 0.07 ppm to higher field in the case of 6b (Table 1).

As the ferrocenyl protons (α-H, β-H) of 6a and 6b show the same chemical shift (Table 1), an electronic effect can be excluded. We explain the NMR data by a shielding effect, owing to an intramolecular π-interaction of the aromatic pyrazolyl pyridine systems. Several similar compounds (1,1'-diarylated ferrocenes) are known in literature [3a-c,11]. Whenever two aromatic substituents at the ferrocene centre are free in rotation around the Fc-Ar bond, they were found to be arranged in a π-stacked geometry. This was proved by single crystal X-ray analysis [3a-c,11] and ^{1}H NMR studies [3c]. The aromatic protons are accordingly shifted to high field while the ferrocenyl protons and all ^{13}C resonances remain uneffected. In contrast, we do not observe any significant high field shift (ca. 0.05 ppm) of the aromatic protons of 4b compared with those of 4a. This may be explained by the free rotation around the pyrazolyl pyridine bond and the steric demand of the two CH$_2$C(O)OCH$_2$CH$_3$ moieties, which can interact with the α-H atoms of the ferrocenyl substituent. Complexation with Mo(CO)$_4$ forces a coplanar arrangement of chelate ligands and decreases the mobility of the alkyl side chains. The X-ray structure of 6a (see Section 2.4) shows that the CH$_2$C(O)OCH$_2$CH$_3$ chain is oriented almost perpendicular to the pyrazolyl plane to prevent steric interaction with the ferrocenyl as well as with the Mo(CO)$_4$ fragment. An equivalent orientation of the second chelate system in 6b would therefore favour a π-interaction. However, variable-temperature ^{1}H NMR measurements of 6a show no splitting of the CH$_2$C(O) protons even at −70 °C. The rotation of the CH$_2$C(O)OEt group and the rotation of the ferrocenyl substituent are therefore fast on the spectroscopic timescale at 400 MHz. In the case of 6b, both CH$_2$C(O) protons give the same NMR resonance at 25 °C. Additionally, the ferrocenyl protons (α-H, α'-H and β-H,

Table 1
^{1}H NMR data of 7, 4a,b and 6a,b

Proton	7	4a	4b	6a	6b	$\delta_{6a}-\delta_{6b}$
4-H	6.92	6.98	6.93	6.95	6.62	0.33
8-H	7.88	7.94	7.92	7.83	7.49	0.34
9-H	7.62	7.69	7.63	7.89	7.66	0.23
10-H	7.11	7.18	7.14	7.30	7.04	0.26
11-H	8.59	8.63	8.59	9.00	8.79	0.21
α-H	—	4.43	4.46	4.50	4.52	0.02
β-H	—	4.31	4.35	4.47	4.50	−0.03

β'-H) are magnetically equivalent. Both observations can only be explained by rotation phenomena, which means that π-stacking is one part of the molecular dynamics of this molecule in solution.

Total assignment of the ^{13}C resonances of **6a** was possible by ^{13}C-^1H correlation spectroscopy (HMQC and HMBC [12]). ^{13}C spin-lattice relaxation time measurements were carried out to study the internal motion of the substituted ferrocene **6a**. The bulky substituent at one of the cyclopentadienyl rings should effectively reduce rotation of this Cp-ring. Simultaneously, relatively free spinning of the unsubstituted ring is allowed [13]. T_1 values were determined from an inversion-recovery pulse sequence, which was applied at 25 °C. Additionally, the ^{13}C-^1H nuclear Overhauser effect was measured for the ^{13}C ferrocene nuclei ($\eta \approx 1.6$ for all protonated Cp nuclei). These NOEs are typical for a dipolar relaxation mechanism. Therefore, paramagnetic relaxation, caused by paramagnetic species (e.g. Fe^{III}, etc.), can be excluded. The T_1 values ($T_1(C-\alpha) = 1.4$ s, $T_1(C-\beta) = 1.1$ s, $T_1(C-Cp) = 4.1$ s) show that the spinning rate of the substituted Cp ring is between 10 and 50 times lower than the spinning of the C_5H_5 ring [13].

2.3. Cyclic voltammetry

In order to probe possible intramolecular electron transfer properties of the compounds described above, cyclic voltammetry was applied [14]. Unsubstituted pyrazolyl pyridine **7**, ferrocenyl substituted ligand **4a**, as well as the respectively coordinated $Mo(CO)_4$ fragments, **8** and **6a**, have been investigated. Voltammetric data are collectively displayed in Table 2. As studies undertaken in acetonitrile (AN) solution appeared to be complicated by solvent interaction of the $Mo(CO)_4$-containing compounds **8** and **6a**, data reported here are

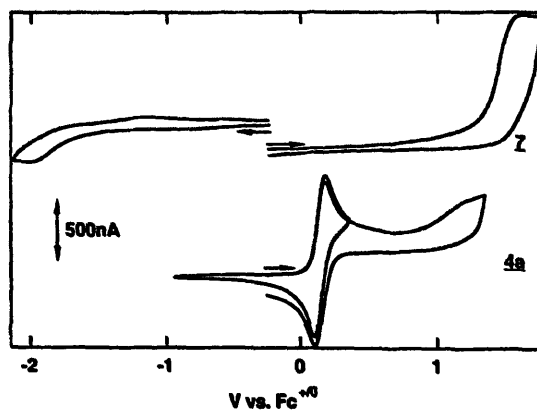Fig. 1. Cyclic voltammetry of **7** and **4a** at 298 K in DCM-0.1 M TBAH. Scan rate 200 mV s⁻¹.

from measurements in the more inert solvent dichloromethane (DCM).

The pyrazoiyl pyridine **7** is electrochemically inactive over a region of about 3 V (Fig. 1). However, at extremes of the available potential range in DCM, an irreversible oxidation and an irreversible reduction process are observed with respective peak potentials (E_p values) of 1.656 V and -2.015 V vs. $Fc^{+/0}$. Accordingly, **7** is not expected to electrochemically interfere with the oxidation of the ferrocenyl and the $Mo(CO)_4$ fragments of the compounds to be discussed in the following.

π-Conjugation of **7** to a cyclopentadienyl ring of ferrocene clearly leads to transfer of electron density from the metal centre to the unsaturated heterocyclic system. The reversible oxidation of substituted ferrocene **4a**, according to Eq. (1), is shifted by $+0.14$ V relative to unsubstituted ferrocene (Fig. 1).

4a is also irreversibly oxidized in a second step at 1.22 V vs. $Fc^{+/0}$. The second oxidation thus leads to

Table 2
Voltammetric data of compounds **4a**, **6a**, **7**, **8**. Potentials for ferrocene redox couple ($Fc^{+/0}$) relative to Ag|0.02 M AgNO₃ in AN; all other potentials in volts vs. $Fc^{+/0}$ couple; scan rate 200 mV s⁻¹

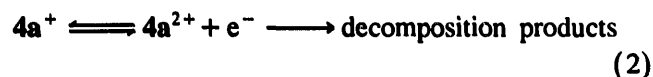| Compound	E_p [a]	E_p [c]	ΔE_p	$E_{1/2}$	Conditions
Fc	0.188	0.114	0.074	0.151	DCM 298 K
	0.150	0.086	0.064	0.118	DCM 243 K
7	1.656	—	—	—	DCM 298 K
	—	−2.015	—	—	DCM 298 K
4a	0.180	0.100	0.080	0.140	DCM 298 K
	1.221	—	—	—	DCM 298 K
8	0.271	—	—	—	DCM 298 K
	−0.199	−0.257	0.058	−0.228	DCM 298 K
6a	0.247	0.203	0.044	0.225	DCM 298 K
	0.311	−0.621	0.932	—	DCM 298 K
		−0.176(ox)			
	0.248	0.181	0.067	0.214	DCM 243 K
	0.358	−0.744	—	—	DCM 243 K
		−0.176(ox)			
	0.248	0.202	0.046	0.228	DCM 243 K [a]

[a] Potential switched after first oxidation wave.
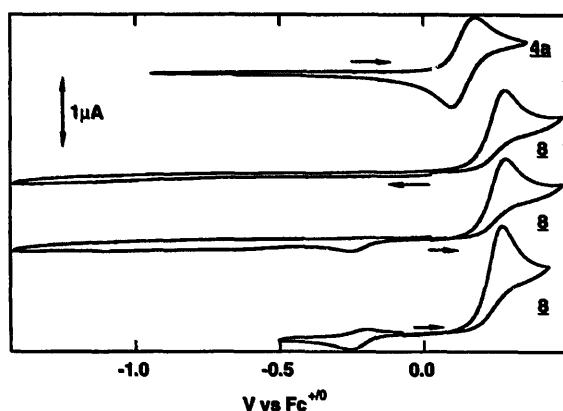
Fig. 2. Cyclic voltammetry of **8** and **4a** at 298 K in DCM-0.1 M TBAH. Scan rate 200 mV s⁻¹.

consumption of **4a⁺**. With respect to the irreversible oxidation of **7**, and the expectedly increased electron density on the ligand system, it seems plausible to attribute the second oxidation wave to ligand-based oxidation of **4a⁺**, followed by decomposition (Eq. (2)).

$$\textbf{4a} \rightleftharpoons \textbf{4a}^+ + e^- \tag{1}$$

$$\textbf{4a}^+ \rightleftharpoons \textbf{4a}^{2+} + e^- \longrightarrow \text{decomposition products} \tag{2}$$

Upon addition of trifluoroacetic acid to the electrolytic solution, the redox potential of **4a** (Eq. (1)) remained constant; this is consistent with ¹H NMR findings of protonation of the pyridine nitrogen, which is well removed from the redox centre, prior to the pyrazole nitrogen. Plenio et al. recently showed, for amino-substituted alkylferrocenes. that the differences of redox potentials of protonated and unprotonated species can be calculated by applying a simple Coulomb point charge model ($\Delta E \sim d^{-1}$) [15]. Protonation of the pyridine nitrogen (d_{Fc-N} ca. 738.8 pm) should therefore not affect the redox potential of the ferrocenyl substituent. No reduction process could be detected for **4a** in the accessible potential range.

The oxidation of **8** in DCM is observed as an irreversible process, which has an E_p value of 0.27 V vs. Fc⁺/⁰ at 298 K (Fig. 2; voltammogram of reversible oxidation of **4a** shown on top for comparison). The process remains irreversible at scan rates up to 1000 mV s⁻¹.

This may be compared [16] to the first irreversible oxidation of (bipy)Mo(CO)₄ (bipy = 2,2'-bipyridyl), which occurs at 0.52 V vs. SCE. On the reverse scan of cyclic voltammograms, a reversible process is observed at $E_{1/2}$ = -0.23 V vs. Fc⁺/⁰ at all applied scan rates (Fig. 2, lower two voltammograms). The ratio of cathodic to anodic peak current for this process strongly depends on the switching potential and scan rate. At 500 mV s⁻¹, i_p^c/i_p^a = 1, and ΔE_p = 0.04 V. Upon multiple cycling between −0.5 and 0.4 V vs. Fc⁺/⁰, the

current associated with the first oxidation wave decreases with increasing scan rates, while the follow-up response increases in magnitude. At a scan rate of 100 to 200 mV s⁻¹, the peak currents of both responses remain essentially constant. This behaviour is consistent with formation of a ligand-stabilized dimeric species $\textbf{8}_2^{2+}$ formed upon oxidation, which is in equilibrium with two molecules of **8**, as outlined in Eq. (3).

$$\textbf{8} \rightleftharpoons \textbf{8}^+ + e^-; 2\textbf{8}^+ \rightleftharpoons \textbf{8}_2^{2+} \tag{3}$$
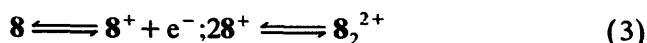
Tom Dieck and Kühl observed dimers linked through side-on coordinated heterounsaturated ligands during voltammetric studies on diazadiene complexes of Mo(CO)₄ in DCM solutions [7a].

When the heterocyclic ligand **7** is now bonded to both ferrocene and Mo(CO)₄ to yield **6a**, the voltammetric response shows some significant changes compared with those observed on **4a** and **8**. At ambient temperature, both metal centres of **6a** are now oxidized at almost the same potential (Fig. 3, top). Lowering the temperature leads to the separation of the two electron transfer steps and an increase in chemical reversibility (Fig. 3, bottom). At room temperature, the product of the second, irreversible oxidation step undergoes chemical changes which lead to additional waves at less positive potentials on reverse and subsequent cycles.

According to the voltammetry of **8** and **4a**, the first process is attributed to the reversible one electron oxidation of the ferrocenyl fragment, while the second process is due to oxidation of the Mo centre. In **6a**, the oxidation potential of the ferrocenyl moiety is shifted by 0.08 V relative to the reversible oxidation of **4a**. The irreversible oxidation of the Mo(CO)₄ group is then observed at a more positive potential than that of the ferrocenyl part since electron density is attracted by the now oxidized and positively charged Fe centre. The peak current ratio of i_p^c/i_p^a = 0.5 at 298 K suggests that two independent electron transfer steps take place during oxidation of **6a**, followed by reduction of only the ferrocenium part upon reversing the potential. Ex-
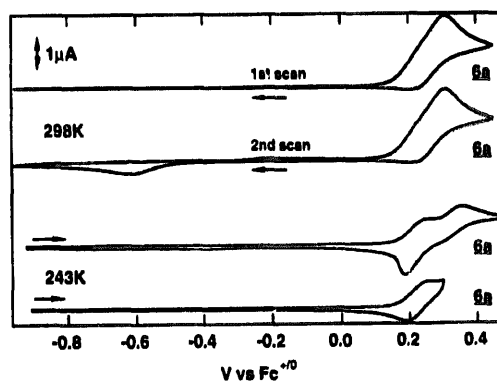

Fig. 3. Cyclic voltammetry of **6a** in DCM-0.1 M TBAH. Scan rate 200 mV s⁻¹. Temperature as marked.

periments undertaken at 243 K support this conclusion, revealing a reversible one electron oxidation at 0.23 V vs. $Fc^{+/0}$, and an almost, but not quite, reversible one electron oxidation at $E_p = 0.36$ V vs. $Fc^{+/0}$. The latter process results in the formation of a new product at room temperature, which is found to be irreversibly reduced at -0.74 V vs. $Fc^{+/0}$, and is followed by an irreversible oxidation step at $E_p = -0.18$ V vs. $Fc^{+/0}$. In the case when the bridging ligand provides a conducting link between the two metal centres, a significant spacing of up to 1.0 V of the two oxidations can be observed [14a,b]. In this situation, the easier to oxidize ferrocenyl part would undergo intramolecular electron transfer after the first oxidation step. Then, at a more positive potential, a second reversible one electron oxidation, again according to oxidation of the Fe centre, is to be expected. However, this is not found with compound 6a, and the results observed are fully consistent

with the two metal centres, Fe and Mo, being insulated from each other by the pyrazolyl pyridine ligand. This behaviour is emphasized by the obvious chemical changes, which follow the second, irreversible oxidation of 6a at room temperature and the oxidation of 8. If one takes the IR spectroscopic data into account, the electron distribution, and thus the redox properties, of 6a are entirely governed by the interaction of ferrocene with the attached heterocyclic ring system, which is expressed in a shift of the redox potential of the ferrocene centre toward positive potentials relative to 4a.

2.4. Crystal structure of 6a

6a crystallizes from CH_2Cl_2-n-pentane as orange prisms in the monoclinic space group $C2/c$ (Int. Tab.-Nr.: 15 [17]). Fig. 4 shows the structure of the molecule in the solid state. Atomic coordinates and isotropic

Table 3
Atomic coordinates and isotropic temperature factors of complex 6a

Atom	x	y	z	U_{iso} [a] ($Å^2$)
Mo(1)	0.36692(2)	0.21207(5)	0.23478(2)	0.0297
Fe(1)	0.41349(2)	0.29701(8)	−0.05763(3)	0.0292
C(1)	0.2902(2)	−0.0582(6)	0.2063(3)	0.0411
C(2)	0.2564(2)	−0.1676(6)	0.1705(3)	0.0406
C(3)	0.2392(2)	−0.1839(6)	0.0988(3)	0.0428
C(4)	0.2561(2)	−0.0877(6)	0.0660(2)	0.0356
C(5)	0.2904(2)	0.0201(5)	0.1051(2)	0.0299
C(6)	0.3131(2)	0.1229(5)	0.0766(2)	0.0269
C(7)	0.3041(2)	0.1474(5)	0.0077(2)	0.0303
C(8)	0.3388(2)	0.2540(5)	0.0134(2)	0.0294
C(9)	0.3082(2)	0.3631(6)	0.2086(2)	0.0300
C(10)	0.3661(2)	0.1829(6)	0.3240(2)	0.0377
C(11)	0.4358(?)	0.0920(7)	0.2730(3)	0.0421
C(12)	0.4199(2)	0.3640(6)	0.2789(2)	0.0354
C(13)	0.4108(2)	0.3921(5)	0.1200(2)	0.0304
C(14)	0.3875(2)	0.5312(6)	0.1217(2)	0.0375
C(15)	0.4159(3)	0.7624(7)	0.1609(4)	0.0793
C(16)	0.4035(3)	0.8457(8)	0.0976(4)	0.0886
C(21)	0.3470(2)	0.3201(6)	−0.0423(2)	0.0296
C(22)	0.3691(2)	0.4512(6)	−0.0439(2)	0.0357
C(23)	0.3669(2)	0.4669(6)	−0.1108(2)	0.0362
C(24)	0.3435(2)	0.3446(6)	−0.1503(2)	0.0407
C(25)	0.3311(2)	0.2537(6)	−0.1090(2)	0.0361
C(31)	0.4725(2)	0.1825(7)	0.0225(3)	0.0490
C(32)	0.4959(2)	0.3043(8)	0.0165(3)	0.0551
C(33)	0.4894(2)	0.3114(9)	−0.0508(4)	0.0596
C(34)	0.4624(3)	0.194(1)	−0.0868(3)	0.0617
C(35)	0.4514(2)	0.1111(7)	−0.0405(4)	0.0447
O(1)	0.3398(1)	0.5557(4)	0.1027(2)	0.0471
O(2)	0.4287(1)	0.6225(5)	0.1494(2)	0.0574
O(9)	0.2804(1)	0.4545(4)	0.1994(2)	0.0463
O(10)	0.3648(1)	0.1646(4)	0.3764(2)	0.0469
O(11)	0.4772(2)	0.0340(5)	0.3013(2)	0.0638
O(12)	0.4517(2)	0.4511(5)	0.3059(2)	0.0545
N(1)	0.3076(1)	0.0357(4)	0.1759(2)	0.0317
N(2)	0.3512(1)	0.2103(5)	0.1229(2)	0.0299
N(3)	0.3672(1)	0.2890(5)	0.0837(2)	0.0298

[a] U_{eq} defined as one third of the trace of the orthogonalized U_{ij} tensor.
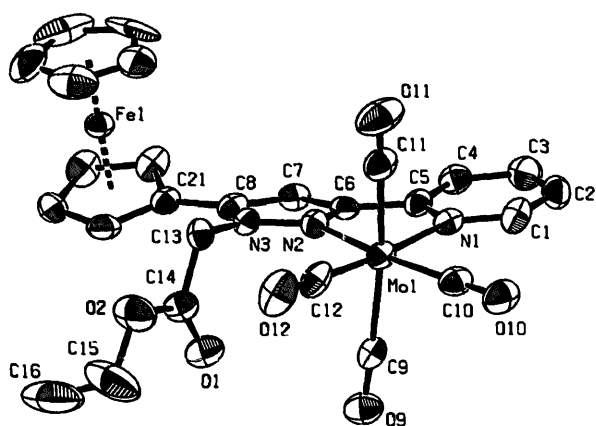
Fig. 4. PLATON [18] plot (50% probability ellipsoids) of the molecular structure of the dinuclear complex 6a.

displacement parameters are presented in Table 3, selected intramolecular distances and angles are summarized in Table 4. The crystal data and collection parameters are given in Table 5.

The molecular structure of the dinuclear complex 6a is dominated by the arrangement of five planes: the pyridine and the pyrazole ring of the chelate ligand backbone, the two cyclopentadienyl rings of the ferrocenyl moiety and the plane, which is defined by N3, C13, C14, O1 and O2. As known from analogous structures [5a,c,19], the pyridine and the pyrazole ring are twisted out of coplanarity. An interplanar angle of 7.9 ° is observed. The cyclopentadienyl ligands of the ferrocenyl moiety are orientated almost coplanar and eclipsed to each other. The angle Cp · -Fe-Cp · (where Cp · is the centre of the plane defined by five C-atoms) is 176.8 °, the distances Cp · -Fe are 1.649 and 1.643 Å.

Table 5
Crystal data and collection parameters for complex 6a

Formula	$C_{26}H_{21}FeMoN_3O_6$
Formula weight	623.3
Colour; habit	orange-brown; brick
Crystal size (mm³)	0.20 × 0.15 × 0.38
Crystal system	Monoclinic
Space group	$C2/c$
a (Å)	27.585(3)
b (Å)	9.655(1)
c (Å)	21.549(3)
β (deg)	119.2(1)
V (Å³)	5010(1)
Z	8
Calculated density (g cm⁻³)	1.6527
μ (cm⁻¹)	11.3
F (000)	2512
Temperature (°C)	−80 ± 1
Scan width (deg)	$0.9 + 0.20° tg\Theta$
Data collection range (deg)	$1.0 < \Theta < 25.0$
Number of reflections collected	9371
Number of unique reflections	4170
Number of reflections for refinement	3084
Observation criteria	$I > 3.0\sigma(I)$
Refined parameters	334
Reflections/parameter	9.23
Final R	0.043
Final R_w	0.0328
Largest remaining feature in the electron density map (e Å⁻³)	+ 1.17; − 1.49

$R = \Sigma(\|F_o| - |F_c\|)/\Sigma |F_o|$; $R_w = [\Sigma w(|F_o| - |F_c|)^2/\Sigma w|F_o|^2]^{1/2}$.

Steric hindrance of the protons in the α-position of the Cp-ring and the methylene group (C13) and the proton at C7 of the pyrazole could be decreased by a perpendicular arrangement of the Cp and the pyrazole ring. In

Table 4
Selected bond lengths (Å) and angles (deg) of complex 6a

Bond lengths			
Mo(1)–C(9)	2.044(5)	Mo(1)–C(10)	1.954(5)
Mo(1)–C(11)	2.026(6)	Mo(1)–C(12)	1.958(6)
Mo(1)–N(1)	2.272(4)	Mo(1)–N(2)	2.233(3)
O(9)–C(9)	1.121(6)	O(10)–C(10)	1.162(5)
O(11)–C(11)	1.144(5)	O(12)–C(12)	1.148(6)
Fe(1)–C(21)	2.030(4)	Fe(1)–C(22)	2.038(5)
Fe(1)–C(23)	2.054(5)	Fe(1)–C(24)	2.041(4)
Fe(1)–C(25)	2.028(4)	Fe(1)–C(31)	2.028(4)
Fe(1)–C(32)	2.045(5)	Fe(1)–C(33)	2.031(5)
Fe(1)–C(34)	2.008(6)	Fe(1)–C(35)	2.019(6)
Bond angles			
C(10)–Mo(1)–C(9)	89.2(2)	C(11)–Mo(1)–C(9)	168.6(2)
C(11)–Mo(1)–C(10)	88.7(2)	C(12)–Mo(1)–C(9)	84.4(2)
C(12)–Mo(1)–C(10)	89.7(2)	C(12)–Mo(1)–C(11)	84.3(2)
N(1)–Mo(1)–C(9)	97.0(2)	N(1)–Mo(1)–C(10)	95.2(2)
N(1)–Mo(1)–C(11)	94.4(2)	N(1)–Mo(1)–C(12)	175.0(2)
N(2)–Mo(1)–C(9)	89.9(2)	N(2)–Mo(1)–C(10)	166.5(2)
N(2)–Mo(1)–C(11)	94.8(2)	N(2)–Mo(1)–N(1)	71.6(1)
O(9)–C(9)–Mo(1)	172.7(4)	O(11)–C(11)–Mo(1)	172.1(5)
O(10)–C(10)–Mo(1)	178.9(4)	O(12)–C(12)–Mo(1)	178.5(5)

addition, an optimal electronic overlap of the π-system demands a coplanar arrangement. The observed inter-planar angle of 20.5 ° fulfils both requests. Minimization of steric hindrance is responsible for the almost perpendicular arrangement of the plane defined by the side chain and the pyrazole ring. As observed in the X-ray structures of other $Mo(CO)_4$ chelate complexes [19b], the axial carbonyl ligands are bent away from the chelate ligand (C9-Mo1-C11 = 168.6(2) °). The axial carbonyl ligands are bent towards the carbonyl ligand in the trans position to the pyridine moiety.

3. Conclusions

Linkage of a ferrocenyl and an $Mo(CO)_4$ moiety by a pyrazolyl pyridine system leads to the bi- and trinuclear complexes 6a,b. The linking pyrazolyl pyridine strongly interacts with the ferrocene part of 6a,b alone, as deduced from ^1H NMR, IR and voltammetric studies. Intramolecular electron transfer via the bridging ligand could not be observed upon electrochemical one electron oxidation of 6a. The heterocyclic bridge acts as an insulator between the Fe and Mo metal centres.

4. Experimental details

The syntheses of all compounds were carried out under an inert gas atmosphere of nitrogen and with dried solvents. The starting materials (η^5-C_5H_4-C(O)CH$_3$)Fe(η^5-C_5H_5) (1a), (η^5-C_5H_4-C(O)CH$_3$)$_2$Fe (1b), $(CO)_4Mo(C_5H_{10}NH)_2$ (5) and $(C_5H_4N$-C$_3H_2N_2$-CH$_2$COOC$_2$H$_5$) (7) were prepared according to literature [5a,9,20]. The NMR (Bruker DPX 400), mass (gas chromatograph Hewlett-Packard HP 5890 coupled with a mass selective detector HP 5970, Finnigan MAT 90), and infrared spectra (Perkin-Elmer 1600 Series FTIR), the X-ray structure analysis (Enraf-Nonius CAD4) of 6a, and all elemental analyses were carried out at Anorganisch-chemisches Institut der Technischen Universität München. The electrochemical investigations were undertaken at the School of Chemistry, La Trobe University (Bundoora, Australia).

4.1. Electrochemistry

A typical solution for electrochemical investigations contained about 1 mM of the substance to be investigated and 0.1 M tetra(n-butyl)ammonium hexafluorophosphate (TBAH) in 5 ml of HPLC grade DCM. DCM was transferred into the electrochemical cell via a column filled with activated neutral alumina. To remove oxygen, the sample solution was then saturated with Ar or N_2 by bubbling through dry inert gas for 15 min. The working electrode was a freshly polished 500 μm diameter Pt disk electrode. An Ag/Ag$^+$ (0.02 M AgNO$_3$

dissolved in AN) reference electrode was used along with a Pt mesh auxiliary electrode to complete the three electrode arrangement. Trifluoroacetic acid was freshly distilled over P_4O_{10} and transferred to the cell under an Ar atmosphere. Compounds were handled under Ar atmosphere and light was excluded during voltammetric experiments. At the end of each set of experiments, a small amount of ferrocene (Fc) was added to the solution and the recorded $E_{1/2}$ value of the Fc$^{+/0}$ couple used to calibrate the cyclic voltammograms. Cyclic staircase voltammograms were recorded using MacLab equipment (EChem® v.1.3.1, MacLab/4e, MacLab P015 potentiostat; all ADInstruments, Sydney, Australia). The applied step height was 1 or 5 mV.

4.2. 2-(5-Ferrocenylpyrazol-3-yl)pyridine (3a) [6]

3a was prepared from 1a, KNH$_2$, and ethyl picolinate (1:2:2 mol equiv.) in liq. NH$_3$-ether followed by ring closure with aqu. N_2H_4-ethanol according to literature [6] in 47% overall yield. Orange microcrystalline solid, m.p. (210 °C, dec.). Analysis. Found: C, 65.05; H, 4.75; N, 12.45. $C_{18}H_{15}FeN_3 \cdot 0.25H_2O$ (333.69) requires: C, 64.79; H, 4.61; N, 12.59%. IR (cm^{-1}, KBr): 3234 (vs, ν_{NH}), 3098 (m), 2959 (w), 2921 (m), 2852 (w), 1602 (m), 1570 (w), 1542 (w), 1487 (w), 1456 (m), 1412 (w), 1170 (w), 1105 (m), 1024 (m), 1001 (m), 814 (s), 782 (s), 730 (w), 531 (m), 514 (w). ^1H NMR (400 MHz, 25 °C, Acetone-d$_6$): δ 12.34 (br, NH), 8.59 (d, $^3J_{10,11}$ = 5.4 Hz, 11-H), 7.97 (br, 8-H), 7.81 (t, $^3J_{8,9}$ = $^3J_{9,10}$ = 7.0 Hz, 9-H), 7.28 (dd, 10-H), 6.98 (s, 4-H), 4.81 (s, 2H, $^3J_{\alpha,\beta}$ < 1.0 Hz, α-H), 4.32 (s, 2H, β-H), 4.09 (s, 5H, Cp-H).

4.3. 1,1'-Bis[3-(2-pyridyl)pyrazol-5-yl]ferrocene (3b)

3b was prepared from 1b, KNH$_2$, and ethyl picolinate (1:4:4 mol equiv.) in liq. NH$_3$-ether followed by ring closure with aqu. N_2H_4-ethanol according to 4.2. in 47% overall yield. Orange microcrystalline solid. 3b is insoluble in all common solvents; NMR data were obtained from DCl solution. Analysis. Found: C, 65.23; H, 4.43; N, 17.46. $C_{26}H_{20}FeN_6 \cdot 0.5H_2O$ (481.35) requires: C, 64.88; H, 4.40; N, 17.46%. IR (cm^{-1}, KBr): 3104 (vs), 3077 (vs), 3031 (vs), 2915 (vs), 2854 (vs), 1596 (vs), 1566 (m), 1475 (m), 1461 (s), 1450 (s), 1414 (s), 1032 (m), 994 (s), 975 (m), 968 (m), 877 (m), 814 (m), 775 (vs), 730 (w), 518 (s). ^1H NMR (400 MHz, 25 °C, DCl): δ 8.43 (d, $^3J_{10,11}$ = 5.5 Hz, 11-H), 8.35 (t, $^3J_{8,9}$ = $^3J_{9,10}$ = 7.5 Hz, 9-H), 7.84 (t, 10-H), 7.70 (d, 8-H), 6.35 (s, 4-H), 4.73 (s, 2H, $^3J_{\alpha,\beta}$ < 1.0 Hz, α-H), 4.38 (s, 2H, β-H).

4.4. [5-Ferrocenyl-3-(2-pyridyl)-1-pyrazolyl]aceticacid-ethylester (4a)

0.89 g (2.70 mmol) 3a were dissolved in 40 ml abs. THF and treated with 0.22 g (5.40 mmol) NaH (60% in

mineral oil). Hydrogen was evolved. After 1 h of stirring 0.60 ml (0.90 g, 5.40 mmol) BrCH$_2$COOEt were added and the mixture stirred for 12 h at room temperature. The volatiles were stripped of in vacuo, the orange residue was washed twice with 30 ml pentane, dissolved in 20 ml ethylacetate, and filtered to separate from NaBr. Evaporation of the solvent gives 0.60 g (1.11 mmol; 54%) of 4a as an orange microcrystalline solid, m.p. (119 °C). Analysis. Found: C, 63.29; H, 5.10; N, 9.83. C$_{22}$H$_{21}$FeN$_3$O$_2$ (415.27) requires: C, 63.63; H, 5.10; N, 10.12%. IR (cm^{-1}, KBr): 3104 (w), 3094 (w), 3085 (w), 3044 (w), 3006 (w), 2983 (m), 2948 (m), 2937 (w), 1748 (vs, C=O), 1595 (m), 1566 (m), 1466 (m), 1456 (s), 1375 (w), 1310 (w), 1206 (vs, C-O), 1024 (m), 824 (w), 781 (s), 505 (m). ^{1}H NMR (400 MHz, 25 °C, CDCl$_3$): δ 8.63 (d, $^3J_{10,11}$ = 4.3 Hz, 11-H), 7.94 (d, $^3J_{8,9}$ = 7.8 Hz, 8-H), 7.69 (t, $^3J_{9,10}$ = 7.5 Hz, 9-H), 7.18 (t, 10-H), 6.98 (s, 4-H), 5.08 (s, N-CH$_2$), 4.43 (br, 2H, $^3J_{\alpha,\beta}$ < 1.0 Hz, α-H), 4.31 (br, 2H, β-H), 4.23 (q, $^3J_{H,H}$ = 7.0 Hz, CH$_2$-CH$_3$), 4.16 (s, 5H, Cp-H), 1.23 (t, CH$_2$-CH$_3$). ^{13}C{^{1}H} NMR (100.625 MHz, 25 °C, CDCl$_3$): δ 168.1 (CO), 152.4 (C-7), 151.3 (C-3), 149.3 (C-11), 143.6 (C-5), 136.5 (C-9), 122.5 (C-10), 120.1 (C-8), 104.5 (C-4), 74.3 (C-i), 69.7 (C-Cp), 69.1 (C-β), 68.3 (C-α), 61.8 (N-CH$_2$), 51.9 (CH$_2$-CH$_3$), 14.1 (CH$_2$-CH$_3$). EI MS (masses with resp. to ^{56}Fe): m/e (%) 415 (100) [M$^+$], 350 (9) [M$^+$-C$_5$H$_5$], 342 (28) [M$^+$-CO$_2$C$_2$H$_5$], 306 (19) [M$^+$-C$_5$H$_5$-OC$_2$H$_4$], 278 (12) [M$^+$-C$_5$H$_5$-O$_2$C$_3$H$_6$], 276 (9) [M$^+$-C$_5$H$_5$-O$_2$C$_3$H$_8$], 121 (9) [(FeC$_5$H$_5$)$^+$], 56 (9) [Fe$^+$].

4.5. 1,1'-Bis{1-[3-(2-pyridyl)pyrazol-5-yl]aceticacidethylester}ferrocene (4b)

4b was prepared from 1.00 g (2.12 mmol) 3b, 0.34 g (8.48 mmol) NaH (60% in mineral oil), and 0.94 ml (1.42 g, 8.48 mmol) BrCH$_2$COOEt in 40 ml abs. THF according to 4.4. in 51% overall yield. Recrystallization from ethylacetate-n-hexane gave the ethylacetate adduct as an orange microcrystalline solid. Analysis. Found: C, 62.46; H, 5.18; N, 11.92. C$_{34}$H$_{32}$FeN$_6$O$_4$·C$_4$H$_8$O$_2$ (732.63) requires: C, 62.30; H, 5.50; N, 11.47%. IR (cm^{-1}, KBr): 3048 (w), 2978 (m), 2960 (w), 2935 (w), 1750 (vs, C=O), 1594 (s), 1566 (m), 1454 (s), 1372 (m), 1309 (w), 1261 (m), 1206 (vs, C-O), 1165 (m), 1024 (s), 786 (s). ^{1}H NMR (400 MHz, 25 °C, CDCl$_3$): δ 8.59 (d, $^3J_{10,11}$ = 4.1 Hz, 11-H), 7.92 (d, $^3J_{8,9}$ = 7.8 Hz, 8-H), 7.63 (t, $^3J_{9,10}$ = 7.3 Hz, 9-H), 7.14 (t, 10-H), 6.93 (s, 4-H), 4.97 (s, N-CH$_2$), 4.46 (br, $^3J_{\alpha,\beta}$ < 1.0 Hz, α-H), 4.35 (br, β-H), 4.18 (q, $^3J_{H,H}$ = 7.1 Hz, CH$_2$-CH$_3$), 1.21 (t, CH$_2$-CH$_3$). ^{13}C{^{1}H} NMR (100.625 MHz, 25 °C, CDCl$_3$): δ 168.0 (CO), 151.8 (C-7), 151.3 (C-3), 149.3 (C-11), 142.4 (C-5), 136.4 (C-9), 122.5 (C-10), 120.2 (C-8), 104.8 (C-4), 75.6 (C-i), 71.3 (C-β), 69.6 (C-α), 61.8 (N-CH$_2$), 51.9 (CH$_2$-CH$_3$), 14.1 (CH$_2$-CH$_3$). CI MS (masses with resp. to ^{56}Fe): m/e (%)

645 (56) [M + H$^+$], 558 (3) [M$^+$-C$_4$H$_6$O$_2$], 512 (20) [M$^+$-C$_4$H$_6$O$_2$-C$_2$H$_6$O], 296 (100) [C$_5$H$_5$-C$_3$HN$_2$(CH$_2$COOC$_2$H$_5$)-C$_5$H$_4$N + H$^+$].

4.6. Tetracarbonyl{[5-ferrocenyl-3-(2-pyridyl)-1-pyrazolyl]aceticacidethylester}molybdenum(0) (6a)

0.21 g (0.51 mmol) 4a and 0.19 g (0.51 mmol) 5 were dissolved in 30 ml abs. toluene and stirred for 3 h at 50 °C. After the evaporation of the solvent in vacuo the orange brown residue was purified by column chromatography on SiO$_2$. Impurities were eluted with Et$_2$O and toluene, 6a was eluted with CH$_2$Cl$_2$. Evaporation of the solvent and recrystallization from CH$_2$Cl$_2$ layered with pentane gave 0.22 g (0.35 mmol, 70%) 6a as orange prisms. Analysis. Found: C, 49.62; H, 3.49; N, 6.58. C$_{26}$H$_{21}$FeMoN$_3$O$_6$ (623.26) requires: C, 50.11; H, 3.40; N, 6.74%. IR (cm^{-1}, toluene): 2017 (s), 1906 (vs), 1883 (vs), 1843 (vs, 4×C=O). IR (cm^{-1}, KBr): 2011 (s), 1892 (vs), 1865 (vs), 1826 (vs, 4×C=O), 1745 (s, C=O$_{Ester}$), 1567 (w), 1446 (w), 1434 (m), 1215 (s, C-O), 778 (m). ^{1}H NMR (400 MHz, 25 °C, CD$_2$Cl$_2$): δ 9.00 (d, $^3J_{10,11}$ = 4.9 Hz, 11-H), 7.89 (dt, $^3J_{8,9}$ = $^3J_{9,10}$ = 7.8 Hz, $^4J_{9,11}$ = 1.5 Hz, 9-H), 7.83 (d, 8-H), 7.30 (ddd, 10-H), 6.95 (s, 4-H), 5.38 (s, N-CH$_2$), 4.50 (t, $^3J_{\alpha,\beta}$ = $^4J_{\alpha,\beta'}$ = 1.1 Hz, α-H), 4.47 (t, β-H), 4.36 (q, $^3J_{H,H}$ = 7.1 Hz, CH$_2$-CH$_3$), 4.25 (s, 5H, Cp-H), 1.36 (t, CH$_2$-CH$_3$). ^{13}C{^{1}H} NMR (100.625 MHz, 25 °C, CD$_2$Cl$_2$): δ 221.8, 221.6 (CO$_{eq.}$), 203.3 (CO$_{ax.}$), 166.6 (CO), 153.0 (C-11), 151.3 (C-7), 150.5 (C-3), 147.0 (C-5), 137.3 (C-9), 123.6 (C-10), 121.1 (C-8), 104.1 (C-4), 72.8 (C-i), 69.9 (C-Cp), 69.9 (C-β), 68.6 (C-α), 62.5 (N-CH$_2$), 52.1 (CH$_2$-CH$_3$), 14.1 (CH$_2$-CH$_3$).

4.7. 1,1'-Bis{{1-[3-(2-pyridyl)pyrazol-5-yl]aceticacidethylester}tetracarbonylmolybdenum(0)}ferrocene (6b)

6b was prepared from 0.37 g (0.50 mmol) 4b and 0.38 g (1.00 mmol) 5 in 30 ml abs. toluene according to 4.6. in 40% overall yield. Purification of 6b by column chromatography is impossible as the compound slowly decomposes in solution. Filtration of the toluene solution over Celite®, evaporation of the solvent in vacuo, and several washings of the solid residue with Et$_2$O lead to a fairly pure, orange-brown, microcrystalline compound. Analysis. Found: C, 48.84; H, 3.74; N, 8.41. C$_{42}$H$_{32}$FeMo$_2$N$_6$O$_{12}$ (1060.48) requires: C, 47.37; H, 3.05; N, 7.90%. IR (cm^{-1}, toluene): 2018 (s), 1907 (vs), 1876 (vs), 1831 (vs, 4×C=O). IR (cm^{-1}, KBr): 2983 (w), 2960 (w), 2935 (w), 2922 (w), 2850 (w), 2016 (s), 1900 (vs), 1873 (vs), 1827 (vs, 4×C=O), 1746 (s, C=O$_{Ester}$), 1608 (w), 1569 (w), 1447 (m), 1437 (m), 1213 (s, C-O), 1024 (m), 781 (m). ^{1}H NMR (400 MHz, 25 °C, CD$_2$Cl$_2$): δ 8.79 (d, $^3J_{10,11}$ = 5.0 Hz, 11-H), 7.66 (dt, $^3J_{8,9}$ = $^3J_{9,10}$ = 8.0 Hz, $^4J_{9,11}$ = 1.5 Hz, 9-H), 7.49 (d, 8-H), 7.04 (dt, 10-H), 6.62 (s, 4-H), 5.25 (s,

N-CH$_2$), 4.52 (t, $^3J_{\alpha,\beta} = {}^4J_{\alpha,\beta'} = 1.5$ Hz, α-H), 4.50 (t, β-H), 4.42 (q, $^3J_{H,H} = 7.0$ Hz, CH$_2$-CH$_3$), 1.42 (t, CH$_2$-CH$_3$). ^{13}C{^{1}H} NMR (100.625 MHz, 25 °C, CD$_2$Cl$_2$): δ 221.5, 221.3 (CO$_{eq}$), 203.5 (CO$_{ax}$), 167.5 (CO), 152.5 (C-11), 150.9 (C-7), 150.4 (C-3), 143.9 (C-5), 137.8 (C-9), 123.5 (C-10), 121.5 (C-8), 105.5 (C-4), 75.9 (C-i), 70.7 (C-β), 70.4 (C-α), 62.9 (N-CH$_2$), 52.3 (CH$_2$-CH$_3$), 14.2 (CH$_2$-CH$_3$).

4.8. Tetracarbonyl[3-(2-pyridyl)-1-pyrazolylaceticacid-ethylester]molybdenum(0) (8)

0.23 g (1.00 mmol) 7 and 0.38 g (1.00 mmol) 5 were dissolved in 30 ml abs. toluene and stirred for 3 h at 50 °C. After the evaporation of the solvent in vacuo the red-brown residue was purified by short column chromatography on silylated SiO$_2$. Impurities were eluted with n-hexane, 8 was eluted with CH$_2$Cl$_2$. Evaporation of the solvent gave 0.35 g (0.80 mmol, 80%) 8 as a red solid. Analysis. Found: C, 46.23; H, 3.88; N, 10.79. C$_{16}$H$_{13}$MoN$_3$O$_6$ (429.24) requires: C, 43.75; H, 2.98; N, 9.57%. IR (cm^{-1}, toluene): 2017 (s), 1906 (vs), 1884 (vs), 1845 (vs, 4×C=O). IR (cm^{-1}, KBr): 2014 (s), 1896 (vs), 1869 (vs), 1824 (vs, 4×C=O), 1753 (s, C=O$_{Ester}$), 1638 (m), 1617 (m), 1439 (m), 1371 (w), 1249 (m), 1215 (m, C-O), 766 (m). ^{1}H NMR (400 MHz, 25 °C, CDCl$_3$): δ 8.97 (d, $^3J_{10,11} = 5.0$ Hz, 11-H), 7.81 (dt, $^3J_{8,9} = {}^3J_{9,10} = 8.0$ Hz, $^4J_{9,11} = 1.5$ Hz, 9-H), 7.71 (d, 8-H), 7.23 (ddd, 10-H), 7.68 (d, $^3J_{4,5} = 3.5$ Hz, 5-H), 6.85 (d, 4-H), 5.21 (s, N-CH$_2$), 4.30 (q, $^3J_{H,H} = 7.0$ Hz, CH$_2$-CH$_3$), 1.31 (t, CH$_2$-CH$_3$). ^{13}C{^{1}H} NMR (100.625 MHz, 25 °C, CD$_2$Cl$_2$): δ 221.7, 221.7 (CO$_{eq}$), 203.3 (CO$_{ax}$), 166.3 (CO), 152.9 (C-11), 151.7 (C-7), 151.3 (C-3), 137.4 (C-9), 135.0 (C-5), 123.7 (C-10), 121.2 (C-8), 104.8 (C-4), 62.6 (N-CH$_2$), 53.9 (CH$_2$-CH$_3$), 14.0 (CH$_2$-CH$_3$).

4.9. Structure determination

Crystal data and details of data collection are summarized in Table 5. Intensity data were recorded on an Enraf-Nonius CAD4 diffractometer, $\lambda = 71.07$ pm (Mo Kα, graphite monochromator). ω-scan mode was used; intensities were corrected for Lorentz, polarization and background effects. For structure solution the metal atoms were located by Patterson techniques [21], all hydrogen atoms were placed in ideal geometry, included in the structure factor calculations but not refined. All calculations were performed on a DECstation 5000/25 using the program CRYSTALS [22].

5. Supplementary material available

A complete list of bond lengths and angles, and tables of hydrogen atom coordinates and thermal param-

References

[1] A. Togni and T. Hayashi (eds.), Ferrocenes, VCH, Weinheim, 1995, pp. 105–168.

[2] (a) W. Kaim and B. Schwederski, Bioanorganische Chemie, B.G. Teubner, Stuttgart, 1991; (b) R. Hahn, Ph. D. Thesis, Technical Univesity of Munich, 1994.

[3] (a) U. Siemeling, U. Vorfeld, B. Neumann and H.-G. Stammler, Chem. Ber., 128 (1995) 481; (b) I.R. Butler, Organometallics, 11 (1992) 74; (c) F. Gelin and R.P. Thummel, J. Org. Chem., 57 (1992) 3780; (d) I.R. Butler, S.J. McDonald, M. Hursthouse and K.M. Abdul Malik, Polyhedron, 14 (1995) 529; (e) B. Farlow, T.A. Nile, J.L. Walsh and A.T. McPhail, Polyhedron, 12 (1993) 2891; (f) I.R. Butler and J.-L. Roustan, Can. J. Chem., 68 (1990) 2212; (g) F. Jäkle, T. Priermeier and M. Wagner, Chem. Ber., 128 (1995) 1163.

[4] H. Brunner and T. Scheck, Chem. Ber., 125 (1992) 701.

[5] (a) W.R. Thiel, M. Angstl and T. Priermeier, Chem. Ber., 127 (1994) 2373; (b) W.R. Thiel, M. Angstl and N. Hansen, J. Mol. Catal., A103 (1995) 5; (c) W.R. Thiel and T. Priermeier, Angew. Chem., 107 (1995) 1870; W.R. Thiel and T. Priermeier, Angew. Chem. Int. Ed. Engl., 34 (1995) 1737.

[6] L. Wolf and H. Hennig, Z. Anorg. Allg. Chem., 341 (1965) 1.

[7] (a) H. tom Dieck and E. Kühl, Z. Naturforsch. b, 37 (1982) 324; (b) J.W. Hershberger, R.J. Klingler and J.K. Kochi, J. Am. Chem. Soc., 104 (1982) 3034.

[8] L.C. Behr, R. Fusco and C.H. Jarboe, in R.H. Wiley (ed.), The Chemistry of Heterocyclic compounds— Pyrazoles, Pyrazolines, Pyrazolidines, Indazoles and Condensed Rings, Interscience, New York, 1967, pp. 10–62.

[9] D.J. Darensbourg and R.L. Kump, Inorg. Chem., 17 (1978) 2680.

[10] L.M. Haines and M.H.B. Stiddard, Adv. Inorg. Radiochem., 12 (1969) 53.

[11] B.M. Foxman, D.D. Gronbeck and M. Rosenblum, J. Organomet. Chem., 413 (1991) 287.

[12] R.R. Ernst, G. Bodenhausen and A. Wokaun, Principles of Nuclear Magnetic Resonance in One and Two Dimensions, Clarendon, Oxford, 1987.

[13] G.C. Levy, Tetrahedron Lett., 35 (1972) 3709.

[14] For example: (a) D. Osella, L. Milone, C. Nervi and M. Ravera, J. Organomet. Chem., 488 (1995) 1; (b) E.E. Bunel, L. Valle, N.L. Jones, P.J. Carroll, C. Barra, M. Gonzalez, N. Munoz, G. Visconti, A. Aizman and J.M. Manriquez, J. Am. Chem. Soc., 110 (1988) 6596; (c) T.-Y. Dong, C.-H. Huang, C.-K. Chang,

H.-C. Hsieh, S.-M. Peng and G.-H. Lee, *Organometallics, 14* (1995) 1776; (d) D. Astruc, *Chem. Rev., 88* (1988) 1189.

[15] H. Plenio, J. Yang, R. Diodone and J. Heintze, *Inorg. Chem., 33* (1994) 4098.

[16] R.J. Crutchley and A.B.P. Lever, *Inorg. Chem., 21* (1982) 2276.

[17] *International Tables of Crystallography*, Vol. I, Kynoch, Birmingham, 1974.

[18] A.L. Spek, The EUCLID package, in D. Sayre (ed.), *Computational Crystallography*, Clarendon, Oxford, 1982, p. 528.

[19] (a) E.O. Schlemper, G.N. Schrauzer and L.A. Hughes, *Polyhedron, 3* (1984) 377; (b) W.A. Herrmann, W.R. Thiel, J.G.

Kuchler, J. Behm and E. Herdtweck, *Chem. Ber., 123* (1990) 1963.

[20] (a) P.J. Graham, R.V. Lindsey, G.W. Parshall, M.L. Peterson and G.M. Whitman, *J. Am. Chem. Soc., 79* (1957) 3416; (b) R.B. Woodward, M. Rosenblum and M. Whiting, *J. Am. Chem. Soc., 74* (1952) 3458.

[21] G.M. Sheldrick, SHELXS-86, *Program for Structure Refinement*, University of Göttingen, Göttingen, 1986.

[22] D.J. Watkin, P.W. Betteridge and J.R. Carruthers, CRYSTALS *User Manual*, Oxford University Computing Laboratory, Oxford, 1986.